

# Tuning the Mechanical Stability of Fibronectin Type III Modules through Sequence Variations

David Craig,<sup>1</sup> Mu Gao,<sup>2</sup> Klaus Schulten,<sup>2</sup> and Viola Vogel<sup>1,\*</sup>

<sup>1</sup>Department of Bioengineering  
University of Washington  
Seattle, Washington 98195

<sup>2</sup>Beckman Institute and  
Department of Physics  
University of Illinois at Urbana-Champaign  
Urbana, Illinois 61801

## Summary

Cells can switch the functional states of extracellular matrix proteins by stretching them while exerting mechanical force. Using steered molecular dynamics, we investigated how the mechanical stability of FnIII modules from the cell adhesion protein fibronectin is affected by natural variations in their amino acid sequences. Despite remarkably similar tertiary structures, FnIII modules share low sequence homology. Conversely, the sequence homology for the same FnIII module across multiple species is notably higher, suggesting that sequence variability is functionally significant. Our studies find that the mechanical stability of FnIII modules can be tuned through substitutions of just a few key amino acids by altering access of water molecules to hydrogen bonds that break early in the unfolding pathway. Furthermore, the FnIII hierarchy of mechanical unfolding can be changed by environmental conditions, such as pH for FnIII<sub>10</sub>, or by forming complexes with other molecules, such as heparin binding to FnIII<sub>13</sub>.

## Introduction

Fibronectin type III modules (FnIII) are structurally ubiquitous, found in 2% of mammalian proteins, and essential to the function of many multimodular proteins. For the extracellular matrix (ECM) protein fibronectin containing more than 15 repeating FnIII modules, it is remarkable that despite high similarity in tertiary structures, the sequence homology for these FnIII modules is conspicuously low, typically less than 20% between modules (Figure 1). By comparison, the sequence homology for the same module across multiple species is uniformly high, approximately 80%–90% between modules, suggesting that the high variability in sequence is essential to function (Hynes, 1990). To a certain extent, some variability in sequence is expected for exposing different FnIII surface chemistries that specify protein-protein interactions. In fact, many of fibronectin's major functions are linked to specific FnIII modules, such as cell binding through the RGD-loop on FnIII<sub>10</sub> (Geiger et al., 2001). However, potential interactions with other proteins do not completely explain the high degree of con-

served sequence variability between FnIII modules nor do they provide an explanation as to why conserved variations occur in amino acids that are buried within modules while in equilibrium.

Recent evidence suggests that nonequilibrium states of FnIII modules may also play a critical role in fibronectin function. Cell stretching of extracellular fibronectin affects fibronectin's functional states and alters the surface chemistry of FnIII modules (Baneyx et al., 2001, 2002; Baneyx and Vogel, 1999; Geiger et al., 2001; Ohashi et al., 2002; Zhong et al., 1998). Variability in the relative mechanical stability of FnIII modules provides a mechanism for controlling their sequential unfolding upon cell stretching of fibronectin (Erickson, 1994). Consistent with this, it has been found that the mechanical stability of native FnIII modules varies several-fold, whereas it varies only slightly for other ECM proteins such as tenascin and titin (Oberdorfer et al., 2000; Oberhauser et al., 1998, 2002). Likewise, experiments with dual-labeled fibronectin undergoing fluorescent resonance energy transfer show a marked reduction in energy transfer for fibronectin incorporated into extracellular matrix fibrils that is consistent with the partial unfolding of FnIII modules upon stretching by cells (Baneyx et al., 2001, 2002). Thus, it is of interest to determine how changes in amino acid sequence that do not significantly affect structure can enhance or weaken the mechanical stability of FnIII modules and to explain how these variations are connected to fibronectin's unique functional properties.

Steered molecular dynamics (SMD) both probes mechanical stability and provides the structural data necessary for elucidating key interactions (Israelowitz et al., 2001). Previous SMD predictions agree well with atomic force microscopy (AFM) results showing that FnIII<sub>10</sub>, containing the cell binding RGD loop, is mechanically one of the least stable FnIII modules (Craig et al., 2001). These SMD results describe the structural events immediately prior to separation of the first  $\beta$  strand from FnIII modules beginning with the breaking of one to two backbone hydrogen bonds connecting the A and B strands. This event is followed by straightening in the A strand, water entering the periphery of the hydrophobic core, and subsequent slipping between the A and G strands such that upper and lower  $\beta$  sheets transition to a state where their  $\beta$  strands are aligned with the external force vector, the so-called aligned state. Finally, breaking of clusters of backbone hydrogen bonds results in the separation of either the A or G strand followed by rapid unraveling of the entire module (Craig et al., 2001; Gao et al., 2002a, 2003; Krammer et al., 1999).

Below we compare the mechanical stability of FnIII modules with known high-resolution structures and provide structural insights into how the variability of single amino acids relates to the mechanical stability of FnIII modules. SMD was used to investigate the early unfolding events for modules FnIII<sub>10</sub>, FnIII<sub>12</sub>, FnIII<sub>13</sub>, FnIII<sub>14</sub>, FnIII<sub>EDB</sub>, and the third FnIII module from the protein tenascin (T-FnIII<sub>3</sub>). We found that SMD protocols adopted

\*Correspondence: vvogel@u.washington.edu

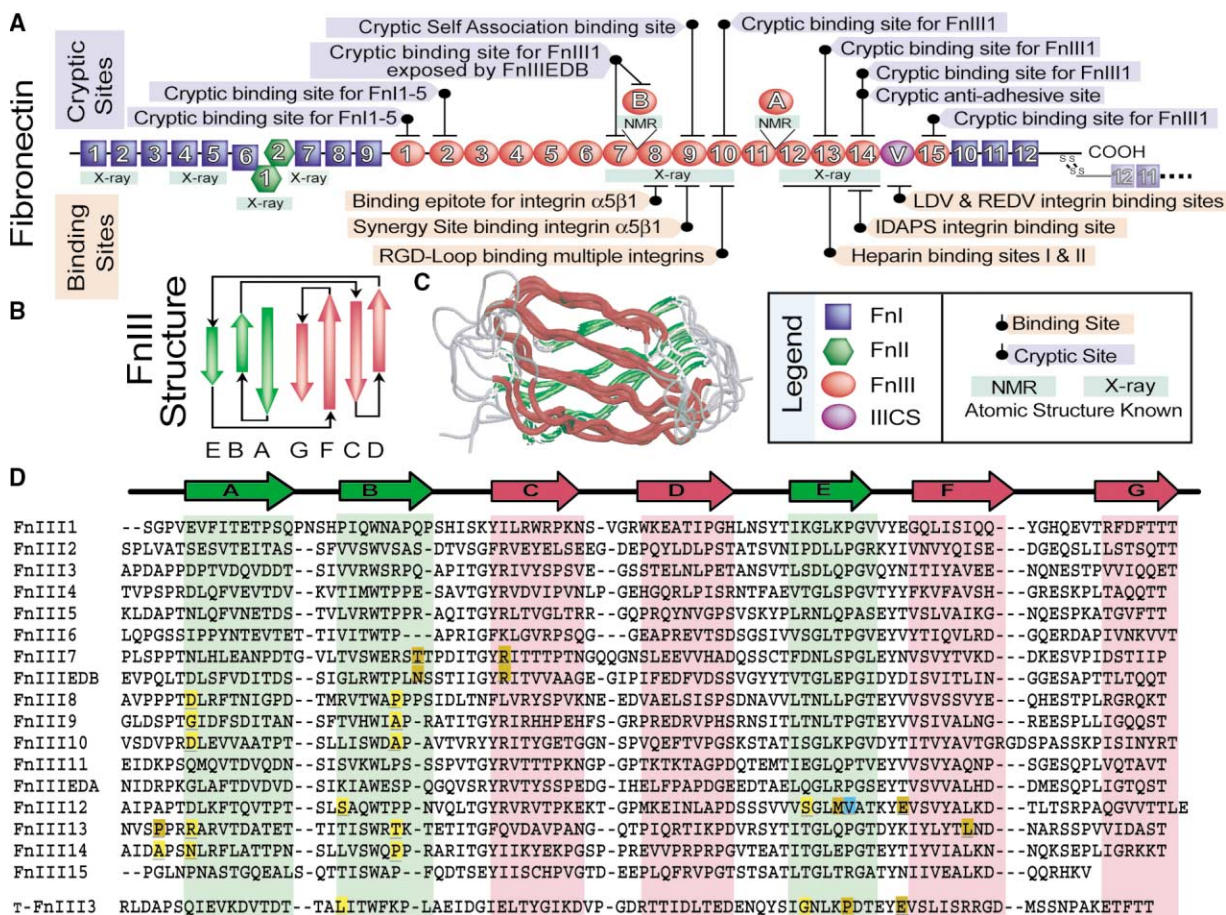


Figure 1. Fibronectin Monomer and FnIII Modules

(A) Schematic of fibronectin emphasizing structural motifs, including Fnl, FnII, and FnIII modules, and highlighting key functional sites (Pankov and Yamada, 2002).  
 (B) The secondary structure for a typical FnIII module. The lower three  $\beta$  strands are shown in green, the upper four  $\beta$  strands in magenta, and loops in gray.  
 (C) Alignment of tertiary structures for modules FnIII<sub>10,12,13,14,EDB</sub> and T-FnIII<sub>3</sub> demonstrating similarity in tertiary structures (coloring is the same as in [B]).  
 (D) Sequences of FnIII modules found in human fibronectin and of T-FnIII<sub>3</sub> of tenascin. Coloring is green for lower  $\beta$  strands and magenta for upper  $\beta$  strands. Amino acids referred to in the text and participating in key hydrogen bonds are highlighted either yellow for backbone bonds or brown for side chain bonds. A key proline substitution is shown in blue.

prior to recent AFM studies correctly predict the mechanical hierarchy for FnIII modules. We further find that while mechanical unfolding ultimately begins with the breaking of a few key backbone hydrogen bonds, amino acid side chains modulate mechanical stability by shielding key hydrogen bonds that break early in the unfolding pathway from attack by water molecules. Our results also indicate that the mechanical hierarchy for FnIII modules can be changed by interaction with the environment. For example, FnIII<sub>10</sub> becomes mechanically more stable as a result of protonation of carboxyl side chains at lower pH, and FnIII<sub>13</sub> becomes more stable as a result of heparin binding. These results suggest a mechanism by which cells can tune the sequence in which FnIII modules undergo structural and thus functional changes during mechanical stretching of fibronectin.

## Results and Discussion

### The Mechanical Hierarchy of FnIII Modules

The relative order of mechanical stability for FnIII modules, defined as mechanical hierarchy, indicates the sequence in which different FnIII modules undergo functional changes when fibronectin is stretched. To determine this hierarchy, modules were stretched under constant force (cf-SMD). Plateaus in time-extension plots obtained from simulations correspond to overcoming unfolding barriers of FnIII modules. The duration of plateaus characterize the strength of barriers and, as expected, the passage time spent in a plateau region increases as force is decreased (see Figure 2) (Izrailev et al., 1997; Lu and Schulten, 1999). Extension through plateaus correlates with the breaking of distinct hydrogen bonds (Lu and Schulten, 2000; Craig et al., 2001)

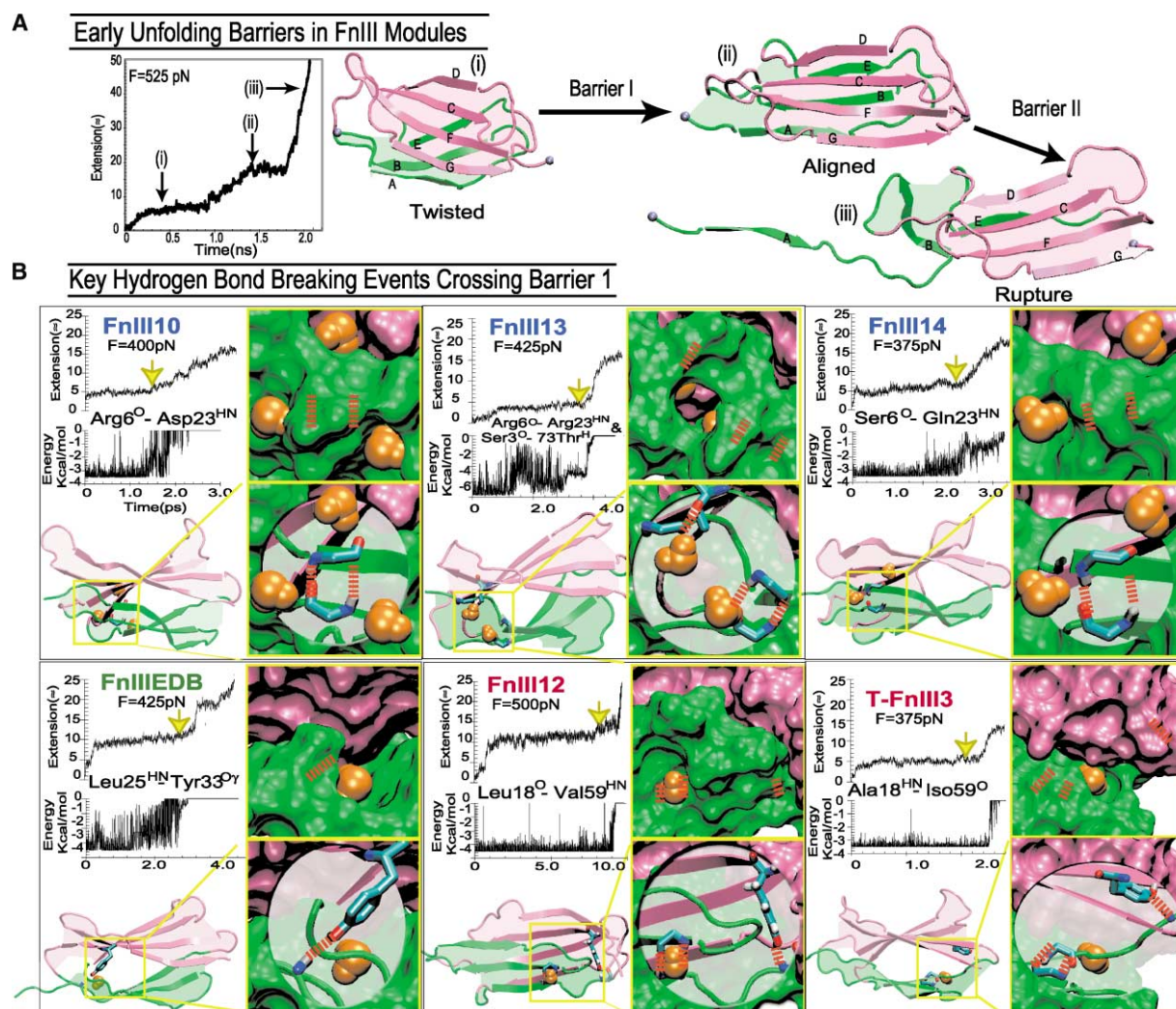


Figure 2. Comparison of the Key Events that Correlate with Crossing of the First Energy Barrier for Different FNIII Modules

(A) The early unfolding pathway of FNIII modules typically exhibits two dominant barriers that are separated by plateaus in time-extension plots prior to unraveling the first  $\beta$  strand.

(B) The first barrier was typically highest for all simulations and its crossing correlated with the breaking of key force bearing hydrogen bonds as a result of increased attack from neighboring water molecules. For modules FnIII<sub>10</sub>, FnIII<sub>13</sub>, FnIII<sub>14</sub>, FnIIIEDB, FnIII<sub>12</sub>, and T-FnIII<sub>3</sub>, the following is shown: a time-extension plot in the upper left, an energy-time plot for key hydrogen bond(s) in the middle left, a snapshot of the FNIII module at the time indicated by the yellow arrow in the lower left, a surface representation of the yellow box illustrating how water approaches the buried hydrogen bonds is shown in the upper right, and a licorice representation of key amino acids cut out of the above surface representation is shown in the lower right. FNIII modules are ordered and labeled based on similarities in barrier crossing events as discussed in the text. Key amino acid side chains are colored by atom (red oxygen, white hydrogen, cyan carbon, and blue nitrogen), key buried hydrogen bonds are red dotted lines, water molecules are orange, the upper  $\beta$  sheet is colored magenta, and the lower  $\beta$  sheet is green.

shown in Figure 2 and discussed in more detail in the next subsection.

SMD simulations provide an approach to predict the mechanical hierarchy of FNIII modules. As shown in Figure 3, distinct differences in mechanical stability are visible when first passage times are plotted versus the applied pulling force. Each data point represents an independent cf-SMD simulation. The mechanically more stable modules are shifted to the right, reflecting longer first passage times to cross the barriers from the twisted to the aligned state (see Figure 2). Overall, even without further quantitative analysis one can immediately ob-

serve the following relative mechanical stability: I27 > FnIII<sub>12</sub> > T-FnIII<sub>3</sub> > FnIII<sub>13</sub>  $\approx$  FnIIIEDB > FnIII<sub>14</sub> > FnIII<sub>10</sub>.

Although in principle it is possible, in practice it is difficult to obtain from MD simulations the detailed shape of the mechanical unfolding barriers (Balsera et al., 1997; Gullingsrud et al., 1999). Recently the Jarzynski equality has been successfully applied to reconstruct a potential of mean force from SMD simulations (Jensen et al., 2002) and quantitative analysis has been provided (Park et al., 2003). However, the construction poses extreme computational demands due to the need of sampling over many trajectories. A systematic reconstruct-

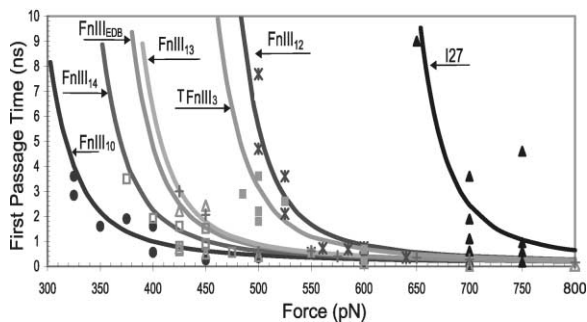


Figure 3. First Passage Time versus Force for FnIII<sub>EDB</sub>, FnIII<sub>10</sub>, FnIII<sub>12</sub>, FnIII<sub>13</sub>, FnIII<sub>14</sub>, T-FnIII<sub>3</sub>, and for Comparison, I27. Data points represent time to cross the first barrier and fitted curves assume a 3 Å barrier width. The stability decreases as follows: I27 > FnIII<sub>12</sub> > T-FnIII<sub>3</sub> > FnIII<sub>13</sub> ≈ FnIII<sub>EDB</sub> > FnIII<sub>14</sub> > FnIII<sub>10</sub>.

tion of the unfolding potential for FnIII modules is not possible at present due to the need of computing many trajectories, but the present results captures the key characteristics of the unfolding barrier along the spatial and the energy scales. For this purpose we use the mean first passage time theory (Izrailev et al., 1997; Schulten et al., 1981) together with dynamic force spectroscopy theory (Evans, 2001) in order to extrapolate from the SMD timescale the mechanical stability of FnIII modules for pulling velocities typical to AFM experiments.

As suggested previously (Izrailev et al., 1997; Lu and Schulten, 1999), the mean first passage time theory relates the potential barrier to the duration of plateaus probed at different forces. By solving the Smoluchowski equation one can determine the mean first passage time  $\bar{\tau}(x_0; F)$  for extending the module from a position  $x_0$  to  $b$  across the barrier  $U(x)$  under a constant force  $F$

$$\bar{\tau}(x_0; F) = \frac{1}{D} \int_{x_0}^b e^{\beta(U(x)-Fx)} dx \int_a^x e^{-\beta(U(y)-Fy)} dy. \quad (1)$$

In this equation,  $\beta = 1/k_b T$ ,  $x$ ,  $y$  denote the reaction coordinate in the interval  $[a, b]$ , and  $D$  is the effective diffusion coefficient. For the present purpose of a simple characterization of the unfolding barrier we assume the saw-tooth potential

$$U(x) = \begin{cases} +\infty & x < a \\ \Delta U(x - a)/(b - a) & a \leq x \leq b. \\ -\infty & x > b \end{cases} \quad (2)$$

Here,  $\Delta U$  is the height of the potential barrier, and  $(b - a)$  corresponds to the width of the barrier. The mean first passage time of interest is  $\tau(F) \equiv \bar{\tau}(x_0 = a; F)$ . The saw-tooth potential inserted into Equation 1 yields the relationship

$$\tau(F) = 2\tau_d \delta(F)^{-2} [e^{\delta(F)} - \delta(F) - 1]. \quad (3)$$

where  $F$  is the externally applied force,  $\tau_d = (b - a)/2D$ , and  $\delta(F) = \beta[\Delta U - F(b - a)]$ . This analytic solution permits one to estimate the barrier height,  $\Delta U$ , from a weighted least-squared fit solving for  $\Delta U$  and  $D$  using plateau duration as a measure of mean first passage time  $\tau$ . The barrier width  $\sim 3.0$  Å is estimated from the

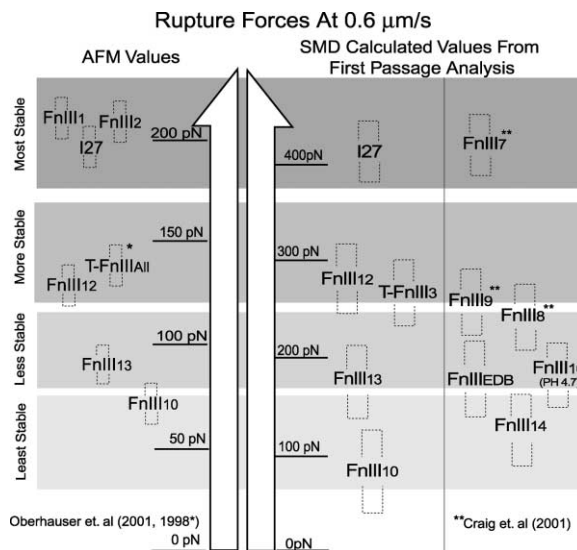


Figure 4. Comparison of Mechanical Stability of FnIII Modules. Comparison of mechanical stability determined by AFM (left) and by SMD as described in Experimental Procedures (right) at a pulling velocity of  $0.6 \mu\text{m/s}$ . Boxes shown surrounding each module indicate error bars from AFM or SMD results ( $3.0 \pm 0.5$  Å). Progressively grayer bars indicate increasing mechanical stability. FnIII modules on the SMD side are grouped by a line to indicate modules that have also been investigated by AFM. AFM results are taken from Oberhauser, et al. (1998, 2002).

extension value during the plateau (Figure 2), a value that corresponds well to results from AFM experiments, for FnIII<sub>13</sub> 3.4 Å (Oberhauser et al., 2002), for FnIII<sub>10</sub> 3.8 Å (Oberhauser et al., 2002), and for I27 2.5 Å (Carrion-Vazquez et al., 1999). A more detailed specification of the unfolding barrier would be inadequate given the fact that the input data taken from single SMD trajectories are extension and duration corresponding to observed plateaus, i.e., solely two values for each module. Figure 3 matches  $\tau$  to the data points for the most prominent plateau of each module sampled. To provide upper and lower bounds for each module's barrier height, the curves were also fitted with a barrier width of 2.5 and 3.5 Å, shown as the upper and lower bounds of the boxes in Figure 4 below.

The most probable rupture force  $f$  for crossing an unfolding barrier is velocity dependent and can be approximated by iteratively solving (Evans, 2001)

$$f \approx f_\beta \ln\left(\frac{v_s}{v_\beta}\right) + f_\beta [\ln(f/f_\beta - 3/2) + (1/2)\ln(f/f_\beta)], \quad (4)$$

where  $v_s$  is the pulling speed and  $b_\beta \equiv k_b T/x_\beta$ ; the quantity  $v_\beta \approx L_p/4\tau_0 \sqrt{x_\beta/b}$  represents the characteristic velocity for pulling a worm-like polymer taut,  $L_p$  is the contour length,  $b$  is the persistence length,  $\tau_0$  is the passage time extrapolated to zero force, and  $x_\beta$  is the barrier width. The contour length and persistence length is assumed to be 28 and 0.4 nm, respectively, consistent with those used in AFM experiments. The variable  $\tau_0$  is determined from Equation 3 with a zero force using the previously determined barrier height.

A quantitative comparison between rupture forces de-

Table 1. Barrier Heights and Rupture Forces Determined by First Passage Time Analysis for Each of the Modules Investigated

	No. SMD Runs: Σ SMD Time	Calc. Barrier Height at Zero Force (kcal/mol)	Calc. Rupture Forces (pN) at 0.6 μm/ps	Hydrogen Bonds
FnIII <sub>10</sub>	15:15 ns	15	50	Arg6(O) <sup>+</sup> -Asp23(HN) <sup>-</sup>
FnIII <sub>10</sub> pH 4.7	6:10 ns	20	150	Arg6(O) <sup>+</sup> -Asp23(HN) <sup>-</sup>
FnIII <sub>12</sub>	11:20 ns	24	230	Leu18(O)-Val59(HN)
FnIII <sub>13</sub>	10:10 ns	19	130	Arg6(O) <sup>+</sup> -Arg23(HN) <sup>+</sup> and Ser3(O)-Thr73(OH)
FnIII <sub>14</sub>	13:17 ns	18	100	Ser6(O)-Iu23(HN) <sup>-</sup>
FnIII <sub>EDB</sub>	8:10 ns	20	140	Leu26(HN)-Tyr33(O)
T-FnIII <sub>3</sub> (1-90)	8:10 ns	23	210	Gln9(HN)-Thr21(O) or Ala18(HN)-Iso59(O)
I-27	12:24 ns	31	390	See (Marszałek et al., 1999)

Key hydrogen bonds corresponding with barrier crossing are highlighted in Figure 1.

lineated from SMD using Equations 3 and 4, and those obtained from AFM data are shown in Figure 4 assuming a pulling velocity of 0.6 μm/s. This velocity corresponds to those used in AFM experiments and is similar to the velocities associated with many cell processes, such as movement of kinesin along a microtubule (Howard et al., 1989). Table 1 summarizes the calculated barrier heights at zero force and the calculated rupture forces at 0.6 μm/s for all the modules simulated here by SMD. It furthermore specifies the key hydrogen bonds that break at the onset of the barrier crossing.

We note that the relative order of mechanical stability for modules investigated by both AFM and SMD agree well. Both AFM and SMD find the relationship: I27 > FnIII<sub>12</sub> > FnIII<sub>13</sub> > FnIII<sub>10</sub>. Partial qualitative agreement is also found between AFM studies of T-FnIII<sub>All</sub> and our SMD simulations of T-FnIII<sub>3</sub>. Here, we find that the mechanical stability of T-FnIII<sub>3</sub> is approximately equal or slightly less than the mechanical stability of FnIII<sub>12</sub>. In comparison, AFM finds an average rupture force for all FnIII modules in tenascin of 137 ± 12 pN similar to the rupture force of 124 ± 18 pN found in separate studies of FnIII<sub>12</sub> (Oberhauser et al., 1999, 2002).

Predicting rupture forces at AFM pulling speeds from SMD requires extrapolating pulling velocities over several orders of magnitude. One cannot expect a uniform scaling behavior over the broad range of velocity linking AFM and SMD (Gao et al., 2002b; Hummer and Szabo, 2003; Lu and Schulten, 1999). It is thus noteworthy that the predicted rupture forces for FnIII modules are within less than an order of magnitude of the rupture forces found in AFM experiments, even if precise quantitative agreement is not yet accomplished. One reason for the lack of quantitative agreement could be that a “saw-tooth” potential that has been assumed to solve Equation 3 is an oversimplification of the actual, but yet unknown, barrier shape.

Since the mean first passage time  $\tau$  is dependent on the detailed shape of the barrier potential, it is of interest to compare impact of different barrier shapes. Figure 5 shows three potentials and corresponding passage time as a function of external force, barrier height or barrier width. Clearly  $\tau$  is dependent on the barrier shape (Figures 5A and 5B). Furthermore, steeper and/or narrower barriers require much longer passage time as shown in Figures 5C and 5D. Nevertheless, we note that for a

particular potential the passage time is monotonous as one changes the applied force. It has been shown that this monotonousness property is not dependent on the shape of the barrier (Izrailev et al., 1997). The duration of passage time, hence, can be used to characterize the relative strength of FnIII modules as long as the same type of barrier shape is assumed. The facts that FnIII modules are structurally highly homologous and have been found to have similar barrier width is consistent with the hypothesis that FnIII modules extend across similar shaped barriers during the earliest stages of unfolding. Indeed, the good agreement between the mechanical hierarchy of FnIII modules predicted by SMD and obtained from AFM studies argues that the largest energy barrier probed by AFM is the same as the one investigated by SMD, i.e., that our analysis of SMD trajectories should yield the same ordering of the mechanical stability (rupture forces) as AFM experiments. In the future, improved computer resources will permit sampling of many trajectories per module, in which case one can accurately reconstruct the barrier shape using the approach in Jensen et al. (2002) and Park et al. (2003) and hopefully achieve quantitative agreement with the AFM experiments.

### Structural Basis for Mechanical Stability

SMD simulations furnish insight into the sequence of structural events that lead to mechanical unfolding. For each FnIII module, the events correlating with plateaus are detailed below and shown in Figure 2. While some simulations were continued until each module was fully unfolded, we will only discuss noteworthy events around the separation of the first  $\beta$  strand.

For all modules, the first significant structural event was the solvation and breaking of one to two conserved backbone hydrogen bonds connecting the A and the B strands. These backbone hydrogen bonds occurred between the 6<sup>th</sup> and 23<sup>rd</sup> amino acids and are next to a conserved proline as the 5<sup>th</sup> amino acid. Breaking of these hydrogen bonds was followed by one or two water molecules entering the periphery of the hydrophobic core, slipping between  $\beta$  sheets such that the  $\beta$  strands align with the external force vector, and finally led to separation of the first  $\beta$  strand. Variability in these events could be correlated to amino acid substitutions and,

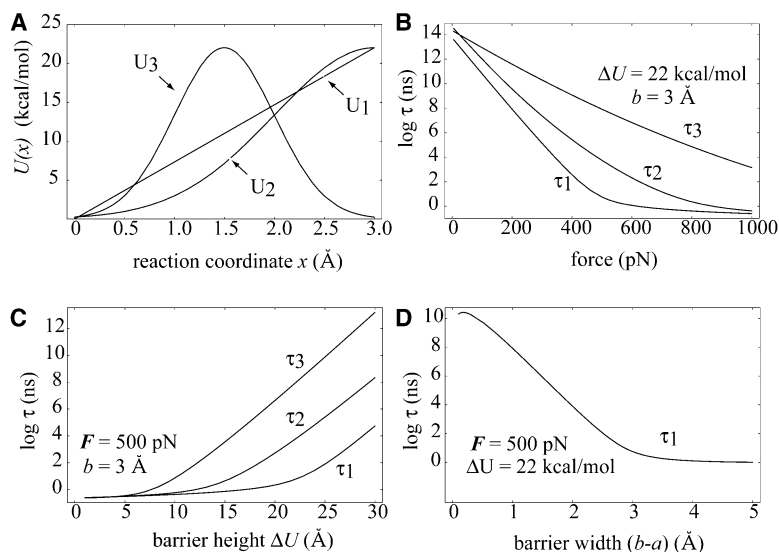


Figure 5. Comparison of the Mean First Passage Time for Three Different Barrier Models Demonstrating the Effect of the Different Barrier Shapes on Mean First Passage Time,  $\tau$  (A)  $U_1(x) = \Delta U (x - a)/(a - b)$ ,  $U_2(x) = \exp[-(x - b)^2/2]$ , and  $U_3(x) = \Delta U \exp[-2(x - b/2)^2]$ , with  $a = 0$ ,  $b = 3 \text{ \AA}$ , and  $\Delta U = 22 \text{ kcal/mol}$ .  $U_1$  corresponds to the saw-tooth model. The mean first passage time  $\tau_i$  for crossing the corresponding barrier  $U_i$  from  $a$  to  $b$  is calculated as a function of externally applied force (B), of barrier height  $\Delta U$  (C), and of barrier width  $(b - a)$  for  $U_i$  (D), all using Equation 1 with a diffusion constant  $D = 1 \text{ \AA}^2/\text{ns}$ , and boundary conditions  $\tau'(a;F) = 0$ ,  $\tau(b;F) = 0$ .

likewise, provided an explanation for observed differences in FnIII mechanical stability.

#### **FnIII<sub>10</sub>**

Crossing the first plateau correlated to the solvation and breaking of the backbone hydrogen bond between Arg6<sup>+</sup> of the A strand and Asp23<sup>-</sup> of the B strand, resulting in a slight straightening of a highly conserved bulge between Pro5 through Asp7<sup>-</sup>. Immediately afterwards, the periphery of the hydrophobic core flanked by Trp23 was solvated, followed by movement of the A and G strands until the  $\beta$  strands of the two sheets appeared approximately aligned. Typically, a second plateau or a region of slow extension (3–7  $\text{\AA}$ ) was observed that ended with the breaking of backbone hydrogen bonds and separation of either the A or G strand (Craig et al., 2001; Gao et al., 2002a).

#### **FnIII<sub>13</sub>**

Similar to FnIII<sub>10</sub>, the unfolding pathway of FnIII<sub>13</sub> contained two significant plateaus in time-extension plots prior to separation of the first  $\beta$  strand, with the first plateau being longest in duration. Crossing the first plateau correlated with the solvation and breaking of the backbone hydrogen bonds between Arg6<sup>+</sup> and Arg23<sup>+</sup> and/or between side chain Tyr73(O<sup>γ</sup>) and Ser3(O). Passage across the second barrier again correlated with separation of either the A or G strand.

#### **FnIII<sub>14</sub>**

Crossing of the first plateau correlated with the breaking of backbone hydrogen bonds between two polar amino acids, Ser6 and Gln23. Crossing of the shorter second plateau correlated with the breaking of several hydrogen bonds connecting the A strand to the rest of the module. If the simulations were continued to full extension, a pronounced intermediate was found later in the unfolding pathway whereby the A and B strands were completely separated while the remainder of the FnIII module remained structurally intact. Similar late-stage intermediates have been previously described for other FnIII modules, although they are typically evident when the FnIII modules were solvated in a large periodic box (Gao et al., 2002a, 2003) or when an implicit water model

was used (Paci and Karplus, 1999, 2000). One functional importance of this intermediate might be that separation of the A and B strands exposes the Pro-Arg-Ala-Arg-Ile (PRARI) sequence at the BC loop which has been implicated in heparin-mediated cell binding (Ingham et al., 1993; Sharma et al., 1999). The physiological importance of the PRARI sequence has been disputed previously since heparin binding was only apparent using peptide fragments and not observed in the fully folded FnIII<sub>14</sub> module (Bloom et al., 1999). These simulations suggest a mechanism by which mechanical force can expose this sequence under physiological conditions.

#### **FnIII<sub>12</sub>**

Unlike the FnIII modules described above, breaking of the Thr6-Thr23 backbone hydrogen bonds and partial solvation of the hydrophobic core did not result in significant extension. Rather, slipping of individual water molecules between the  $\beta$  strands was prevented by an additional hydrogen bond between Met63 and Tyr68. The added stability likely resulted from substitution of a highly conserved proline to Val64 adding flexibility in the E-F loop and allowing for formation of a second hydrogen bond between Met63 and Tyr68. A proline is found at this position for all other fibronectin FnIII modules with the exceptions of FnIII<sub>12</sub> and FnIII<sub>15</sub> (highlighted in blue in Figure 1).

#### **T-FnIII<sub>3</sub>**

Similar to FnIII<sub>12</sub>, breaking of the Ser6 and Phe23 hydrogen bonds resulted in solvation of the periphery of the hydrophobic core but did not result in significant extension. Also similar to FnIII<sub>12</sub>, the  $\beta$  strand alignment was prevented by a hydrogen bond between Tyr68 and Lys63<sup>+</sup> that linked the upper and lower  $\beta$  sheets. Extension beyond the longest plateau correlated with the solvation and breakage of either Gln8(HN)-Thr20(O) or Ala18(HN)-Iso59(O). Previous experimental studies have found that extending the 90 amino acid T-FnIII fragment used for the crystal structure by two residues, referred to as T-FnIII(1-92), resulted in thermodynamic stabilization of the module (Hamill et al., 1998; Meekhof et al., 1998). Using the extended T-FnIII<sub>3</sub>(1-92) modeled from

previously published NMR data (Meekhof et al., 1998), these additional residues did not appear to substantially affect the duration of the first plateau in SMD. For example, for T-FnIII<sub>3</sub>(1-92) the first plateau extended for 3.5 ns at 500 pN and 0.7 ns at 550 pN, slightly longer than 2.5 ns at 500 pN and 0.6 ns at 550 pN for T-FnIII<sub>3</sub>(1-90). This result is consistent with other observations that mechanical and thermodynamic stability are not necessarily correlated since the unfolding might occur along different trajectories (Best et al., 2001; Carrion-Vazquez et al., 1999).

#### ***FnIII<sub>EDB</sub>***

Unlike other FnIII modules investigated, FnIII<sub>EDB</sub> does not contain a proline at the fifth amino acid and, as predicted from the observations made above, the hydrogen bond between Thr6 and Thr23 broke without a major plateau. Noteworthy, absence of the proline at the fifth position in FnIII modules has been linked to FnIII aggregation, though the detailed mechanism is unclear (Steward et al., 2002). Thus, one possible role for the proline at the fifth amino acid is to stabilize the 6–23 hydrogen bonds. For FnIII<sub>EDB</sub>, further extension was prevented by a single side chain hydrogen bond connecting the upper and lower  $\beta$  sheets between Tyr33 and Leu26. A similar hydrogen bond involving a tyrosine side chain had also been found to substantially increase the mechanical stability of FnIII<sub>7</sub> (Craig et al., 2001) as it locks the  $\beta$  sheets in place thus preventing the alignment of their  $\beta$  strands with the external force vector. In FnIII<sub>EDB</sub>, however, the stabilizing contribution of this hydrogen bond is less than in FnIII<sub>7</sub> due to the proline substitution and easier solvent access to Tyr33 and Leu26.

#### ***Comparison***

Common themes emerge when comparing the structural origins of mechanical stability in FnIII modules. The mechanical stability of FnIII modules is related to how well key hydrogen bonds that break early in the unfolding pathway are shielded from attack by water molecules. In FnIII<sub>7</sub> (Craig et al., 2001), FnIII<sub>12</sub>, FnIII<sub>EDB</sub>, and T-FnIII<sub>3</sub>, hydrogen bonds buried in the hydrophobic core between the O $\gamma$  atom of a tyrosine in the upper  $\beta$  sheets and a HN backbone atom in the lower  $\beta$  sheets prevented alignment of the  $\beta$  strands with the external force vector even when parts of the hydrophobic core had been solvated. In particular, for FnIII<sub>12</sub>, this tyrosine hydrogen bond appeared to be even further stabilized by a lower solvent accessibility, apparently resulting from the absence of a proline at position 64. Second, it was found that amino acid side chains, particularly those containing charged side groups contacting the 6<sup>th</sup> and 23<sup>rd</sup> amino acid in the A and B strands respectively, lowered mechanical stability by shielding key backbone hydrogen bonds from attack by water molecules. For example, the mechanical stability of FnIII<sub>10</sub> containing charged amino acids between the Arg6<sup>+</sup> and Asp23<sup>-</sup> amino acids was considerably lower than that of other FnIII modules not containing similarly charged amino acids. This finding is investigated in more detail in the next section.

#### **The Mechanical Stability of FnIII<sub>10</sub> Is pH Dependent**

Previous experimental and SMD studies agree in that FnIII<sub>10</sub> is one of the mechanically weakest modules de-

spite having an essential role in cell binding and the formation of a mechanically stable complex (Craig et al., 2001; Oberhauser et al., 2002). In contrast to mechanical weakness, FnIII<sub>10</sub> has high thermodynamic stability (Cota and Clarke, 2000). Recently, Koide et al. found that FnIII<sub>10</sub> becomes even more thermodynamically stable at  $\sim$ pH 4.7 as a result of protonation of three negative amino acids: Asp7<sup>-</sup>, Asp23<sup>-</sup>, and Glu9<sup>-</sup> (Koide et al., 2001). While mechanical stability does not necessarily correlate with thermodynamic stability (Best et al., 2001; Carrion-Vazquez et al., 1999), this finding was intriguing since these amino acids also play a key role in protecting hydrogen bonds between R6<sup>+</sup> and Asp23<sup>-</sup> from attack by water molecules.

We conducted additional SMD simulations of FnIII<sub>10</sub> with Asp7<sup>-</sup>, Asp23<sup>-</sup>, and Glu9<sup>-</sup> neutralized by protonation to determine the effect of a lower pH on mechanical stability. It was immediately found during thermalization and equilibration that a new side chain hydrogen bond formed between the protonated carboxyl groups of Asp23 and Asp7. During a 1 ns equilibration of FnIII<sub>10</sub> at a pH of approximately 4.7, this new hydrogen bond would stochastically break and the side chains of Asp7 and Glu9 would temporarily come closer (see Figure 6). This finding is particularly interesting because the side chains of these amino acids are partially separated during equilibration of neutral pH FnIII<sub>10</sub> due to the repulsive interactions of these three negative side groups. In SMD simulations, the first passage times for FnIII<sub>10</sub> became significantly longer at lower pH and the barrier height increased by roughly 33%, from 15 to 20 kcal/mol. As a result, the mechanical stability of FnIII<sub>10</sub> rises from being the least stable of the FnIII modules tested here to being even more stable than FnIII<sub>3</sub>. Further stabilization may result from conformational changes occurring beyond the timescale of molecular dynamics equilibration.

The finding that FnIII<sub>10</sub> is mechanically more stable at lower pH may have physiological relevance. Lower extracellular pH is associated with cells in stressed environments, such as in wound and cancer tissues where measurements of the bulk pH are approximately 6–7 and 5–6, respectively (Crowther et al., 2001; Rofstad, 2000). Additionally, fibronectin is known to play a key role in bone resorption which is also associated with a reduction in pH to the surrounding environment (Bushinsky and Frick, 2000). The pH of the microenvironment immediately neighboring FnIII<sub>10</sub> will be lowered further due to the overall negative charge found on modules FnIII<sub>7-10</sub> and as a result of local pH gradients. Finally, the three negative residues involved in the thermal (Koide et al., 2001) and mechanical stabilization of FnIII<sub>10</sub> are highly conserved and unique to FnIII<sub>10</sub> across multiple organisms, consistent with their predicted functional importance in regulating the mechanical stability of FnIII<sub>10</sub>.

#### **SMD Structural Analysis Suggests Heparin Binding Mechanically Stabilizes FnIII<sub>13</sub>**

FnIII<sub>13</sub> contains a heparin binding site, Hep-II, that is required for inducing stress fibers and formation of focal contacts (Bloom et al., 1999). Recent studies mapping the Hep-II binding site find that heparin binding to FnIII<sub>13</sub> involves interactions with the first 29 amino acids includ-

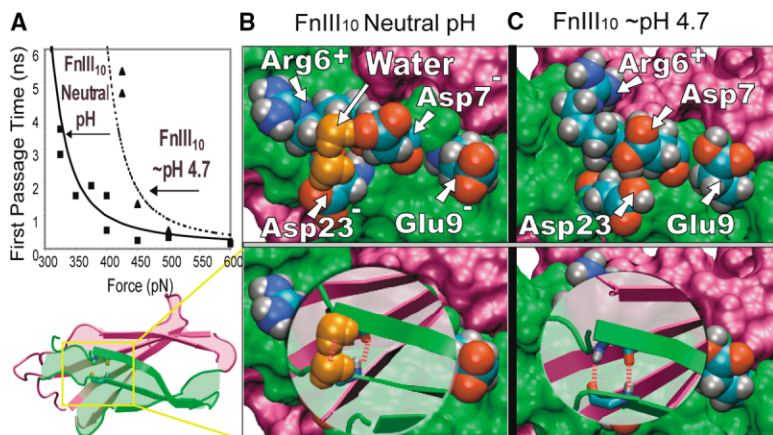


Figure 6. FnIII<sub>10</sub> was Found to be Mechanically More Stable at Low pH

(A) First passage time versus force for FnIII<sub>10</sub> simulated at neutral pH and ~pH 4.7.

(B) In simulations at neutral pH, the negative interactions of the carboxyl side groups for amino acids Asp7, Asp23, and Glu9 resulted in the separation of the side chains exposing the force bearing Arg6(O) to Asp23(HN) backbone hydrogen bonds to water molecules.

(C) Protonation of Asp7, Asp23, and Glu9, consistent with ~pH 4.7, resulted in the side groups blocking access of water molecules to the Arg6(O) to Asp23(HN) backbone hydrogen bond. In the snapshots shown, only Arg6, Asp7, Asp23, Glu9, and key water molecules are presented explicitly: oxygen atoms are colored red, hydrogen atoms are white, carbon atoms are cyan, nitrogen atoms are blue, water molecules are orange, the upper β sheet is magenta, and the lower β sheet is green.

ing six positive amino acids that form a cationic cradle (Bloom et al., 1999; Busby et al., 1995; Sachchidanand et al., 2002; Sharma et al., 1999).

Notably, these same amino acids involved in heparin binding also play key roles in the early stages of unfolding. Unfolding of FnIII<sub>13</sub> begins with separation of the A and B strands containing 25 of the first 29 previously mentioned amino acids. More specifically, the amino acids involved in the formation of key force bearing hydrogen bonds between Ser3 and Thr73, and Arg6<sup>+</sup> and Arg23<sup>+</sup>, as identified by SMD, were also found to undergo significant NMR chemical shifts upon heparin binding (Ser3, Arg6<sup>+</sup>, Arg23<sup>+</sup>), indicating a decrease in their solvent exposure. This is consistent with measurements indicating that heparin binding to FnIII<sub>13</sub> is entropically driven with a high energy of solvation. Further mutagenesis studies also identified Arg6<sup>+</sup> and Arg7<sup>+</sup> to be necessary for heparin binding (Sachchidanand et al., 2002). Taken together, it is likely that binding of heparin to this Hep-II site prevents water molecules from attacking the force bearing hydrogen bonds between Arg6<sup>+</sup> and Arg23<sup>+</sup>. If complexation limits the access of water molecules to these backbone hydrogen bonds, it is expected that heparin binding to FnIII<sub>13</sub> stabilizes the FnIII<sub>13</sub> module.

### Conclusions

Determination of the mechanical hierarchy in which FnIII modules unfold if mechanically stretched is essential to learn how cells use force to regulate the exposure of molecular recognition sites by stretching extracellular matrix proteins. Our SMD predictions regarding the hierarchy in which FnIII modules unfold agree well with experimental findings performed by atomic force microscopy. Here we explain how single amino acid changes, or even the protonation of single carboxyl groups in FnIII<sub>10</sub>, alter the accessibility of water to key backbone or backbone-side chain hydrogen bonds that break early in the unfolding pathway. Identification of amino acids that regulate the mechanical stability of FnIII modules provides novel functional explanations into why the sequence homology of FnIII modules is low despite their

remarkable structural similarities. Our data further suggest that the mechanical hierarchy of unfolding is not strictly given by the amino acid sequence but can be regulated by the local environment and by complex formation with other molecules. For example, for FnIII<sub>10</sub>, we found that protonation of the carboxyl groups of Asp7, Glu9, and Asp23, corresponding to a lowered pH, can substantially increase the first major energy barrier contributing to its mechanical stability. Furthermore, insights into the role played by key residues in the early unfolding events suggest that heparin binding to FnIII<sub>13</sub> will increase its mechanical stability. Consequently, our studies imply that the mechanical stability of FnIII modules involved in cell binding can be altered in response to environmental changes. Our results also uncover novel structural principles that regulate mechanical stability: variations in the mechanical stability of different proteins depend not simply on the pattern of backbone hydrogen bonds, but more critically on how well key hydrogen bonds are shielded from attack by water molecules. Taken together with the known biological functions of fibronectin, these results suggest how subtle variations in amino acid sequence can have a profound effect on protein function and ultimately cellular behavior.

### Experimental Procedures

SMD simulations were used to probe the mechanical properties of FnIII modules under force. Using the program NAMD (Nelson, 1996), molecular dynamic simulations were carried out on an all-atom model of individual FnIII modules with the CHARMM22 force field (MacKerell, 1998) and including explicit solvent described by TIP3P (Jorgensen, 1983) water parameters. Forced unfolding was accomplished by adding a constant force to the C<sub>α</sub> atom of the carboxy terminus along the direction of the vector connecting the two termini while the amino terminus was held fixed. Modules were solvated in a sphere of explicit water molecules with a radius of 32 Å, resulting in approximately 13,000 atoms so as to be consistent with previous studies and allow for good sampling per module (Craig et al., 2001; Krammer et al., 1999). Single FnIII modules were adopted from known X-ray crystallographic or NMR structures. FnIII<sub>10</sub> was adopted from the FN-III<sub>7-10</sub> fragment (PDB code 1FNF) (Leahy et al., 1996). FnIII<sub>12</sub>, FnIII<sub>13</sub>, and FnIII<sub>14</sub> were adopted from the FnIII<sub>2-14</sub> fragment (PDB code 1FNH) (Sharma et al., 1999). An extended version of T-FnIII<sub>3</sub> was modeled by adding two amino acids to the carboxy

terminus using published NMR data (Meekhof et al., 1998). FnIII<sub>EDB</sub> was adopted from PDB code 2FNB (Fattorusso et al., 1999) and T-FnIII<sub>3</sub> from PDB code 1TEN (Leahy et al., 1992). Simulations were also conducted on I27 to provide further comparison to AFM studies (Lu et al., 1998). A total of ~85 SMD simulations encompassing together ~175 ns were conducted. Each nanosecond of simulation utilized ~200 CPU hours on Beowulf clusters of either 12 or 36 Athlon 1.2 GHz Processors.

Forces were applied to single FnIII modules ranging from 300 to 1000 pN. Extension is defined as the difference in end-to-end distance between equilibrated and stretched structures. Time-extension plots clearly showed plateaus early in the unfolding pathway. The unfolding barrier height,  $\Delta U$ , is determined from Equation 3 using a weighted least-squared fit solving for  $\Delta U$  and  $D$ , with a barrier width of 3.0 Å and using plateau duration as a measure of mean first passage (barrier crossing) time  $\tau$ . In some cases, barriers appeared less as distinct plateaus but more as regions of gradual extension due to straightening of the termini. In these cases, we analyzed changes in hydrogen bonding patterns, side-chain contacts, van der Waals (VDW) energies,  $\phi/\psi$  angles, and solvent accessibility to identify a distinct event correlating with barrier crossing consistent with the other simulations. The most probably rupture force was determined by iteratively solving Equation 4.

#### Acknowledgments

This work was supported by the National Institutes of Health (NIH PHS5P41RR05969 and I-ROIGM60946 [K.S.], 8-R01EB00249-09 [V.V.], and 5T32GM08268 [D.C.]), a graduate award through a University of Washington Initiative Fund (UIF [D.C.]), and the National Science Foundation (NRAC MCA93S028 [K.S.]).

Received: May 16, 2003

Revised: September 4, 2003

Accepted: September 16, 2003

Published: January 13, 2004

#### References

Balsera, M., Stepaniants, S., Izrailev, S., Oono, Y., and Schulten, K. (1997). Reconstructing potential energy functions from simulated force-induced unbinding processes. *Biophys. J.* **73**, 1281–1287.

Baneyx, G., and Vogel, V. (1999). Self-assembly of fibronectin into fibrillar networks underneath dipalmitoyl phosphatidylcholine monolayers: role of lipid matrix and tensile forces. *Proc. Natl. Acad. Sci. USA* **96**, 12518–12523.

Baneyx, G., Baugh, L., and Vogel, V. (2001). Coexisting conformations of fibronectin in cell culture imaged using fluorescence resonance energy transfer. *Proc. Natl. Acad. Sci. USA* **98**, 14464–14468.

Baneyx, G., Baugh, L., and Vogel, V. (2002). Supramolecular Chemistry And Self-assembly Special Feature: Fibronectin extension and unfolding within cell matrix fibrils controlled by cytoskeletal tension. *Proc. Natl. Acad. Sci. USA* **99**, 5139–5143.

Best, R.B., Li, B., Steward, A., Daggett, V., and Clarke, J. (2001). Can non-mechanical proteins withstand force? Stretching barnase by atomic force microscopy and molecular dynamics simulation. *Biophys. J.* **81**, 2344–2356.

Bloom, L., Ingham, K.C., and Hynes, R.O. (1999). Fibronectin regulates assembly of actin filaments and focal contacts in cultured cells via the heparin-binding site in repeat III13. *Mol. Biol. Cell* **10**, 1521–1536.

Busby, T.F., Argraves, W.S., Brew, S.A., Pechik, I., Gilliland, G.L., and Ingham, K.C. (1995). Heparin binding by fibronectin module III-13 involves six discontinuous basic residues brought together to form a cationic cradle. *J. Biol. Chem.* **270**, 18558–18562.

Bushinsky, D.A., and Frick, K.K. (2000). The effects of acid on bone. *Curr. Opin. Nephrol. Hypertens.* **9**, 369–379.

Carrion-Vazquez, M., Oberhauser, A.F., Fowler, S.B., Marszalek, P.E., Broedel, S.E., Clarke, J., and Fernandez, J.M. (1999). Mechanical and chemical unfolding of a single protein: a comparison. *Proc. Natl. Acad. Sci. USA* **96**, 3694–3699.

Cota, E., and Clarke, J. (2000). Folding of beta-sandwich proteins: three-state transition of a fibronectin type III module. *Protein Sci.* **9**, 112–120.

Craig, D., Krammer, A., Schulten, K., and Vogel, V. (2001). Comparison of the early stages of forced unfolding for fibronectin type III modules. *Proc. Natl. Acad. Sci. USA* **98**, 5590–5595.

Crowther, M., Brown, N.J., Bishop, E.T., and Lewis, C.E. (2001). Microenvironmental influence on macrophage regulation of angiogenesis in wounds and malignant tumors. *J. Leukoc. Biol.* **70**, 478–490.

Erickson, H.P. (1994). Reversible unfolding of fibronectin type III and immunoglobulin domains provides the structural basis for stretch and elasticity of titin and fibronectin. *Proc. Natl. Acad. Sci. USA* **91**, 10114–10118.

Evans, E. (2001). Probing the relation between force—lifetime—and chemistry in single molecular bonds. *Annu. Rev. Biophys. Biomol. Struct.* **30**, 105–128.

Fattorusso, R., Pellicchia, M., Viti, F., Neri, P., Neri, D., and Wuthrich, K. (1999). NMR structure of the human oncofoetal fibronectin ED-B domain, a specific marker for angiogenesis. *Struct. Fold. Des.* **7**, 381–390.

Gao, M., Craig, D., Vogel, V., and Schulten, K. (2002a). Identifying unfolding intermediates of FN-III(10) by steered molecular dynamics. *J. Mol. Biol.* **323**, 939–950.

Gao, M., Lu, H., and Schulten, K. (2002b). Unfolding of titin domains studied by molecular dynamics simulations. *J. Muscle Re. Cell Mot.* **23**, 513–521.

Gao, M., Craig, D., Lequin, O., Campbell, I.D., Vogel, V., and Schulten, K. (2003). Structure and functional significance of mechanically unfolded fibronectin type III1 intermediates. *Proc. Natl. Acad. Sci. USA* **100**, 14784–14789.

Geiger, B., Bershadsky, A., Pankov, R., and Yamada, K.M. (2001). Transmembrane crosstalk between the extracellular matrix and the cytoskeleton. *Nat. Rev. Mol. Cell Biol.* **2**, 793–805.

Gullingsrud, J.R., Braun, R., and Schulten, K. (1999). Reconstructing potentials of mean force through time series analysis of steered molecular dynamics simulations. *J. Comput. Phys.* **151**, 190–211.

Hamill, S.J., Meekhof, A.E., and Clarke, J. (1998). The effect of boundary selection on the stability and folding of the third fibronectin type III domain from human tenascin. *Biochemistry* **37**, 8071–8079.

Howard, J., Hudspeth, A.J., and Vale, R.D. (1989). Movement of microtubules by single kinesin molecules. *Nature* **342**, 154–158.

Hummer, G., and Szabo, A. (2003). Kinetics from nonequilibrium single-molecule pulling experiments. *Proc. Natl. Acad. Sci. USA* **97**, 6521–6526.

Hynes, R.O. (1990). *Fibronectins* (New York: Springer-Verlag).

Ingham, K.C., Brew, S.A., Migliorini, M.M., and Busby, T.F. (1993). Binding of heparin by type III domains and peptides from the carboxy terminal hep-2 region of fibronectin. *Biochemistry* **32**, 12548–12553.

Israilewitz, B., Gao, M., and Schulten, K. (2001). Steered molecular dynamics and mechanical functions of proteins. *Curr. Opin. Struct. Biol.* **11**, 224–230.

Izrailev, S., Stepaniants, S., Balsera, M., Oono, Y., and Schulten, K. (1997). Molecular dynamics study of unbinding of the avidin-biotin complex. *Biophys. J.* **72**, 1568–1581.

Jensen, M.O., Park, S., Tajkhorshid, E., and Schulten, K. (2002). Energetics of glycerol conduction through aquaglyceroporin GlpF. *Proc. Natl. Acad. Sci. USA* **99**, 6731–6736.

Jorgensen, W.L., Chandrasekhar, J., Madura, J.D., Impey, R.W., and Klein, M.L. (1983). Comparison of simple potential functions for simulating water. *J. Chem. Phys.* **79**, 926–935.

Koide, A., Jordan, M.R., Horner, S.R., Batori, V., and Koide, S. (2001). Stabilization of a fibronectin type III domain by the removal of unfavorable electrostatic interactions on the protein surface. *Biochemistry* **40**, 10326–10333.

Krammer, A., Lu, H., Israilewitz, B., Schulten, K., and Vogel, V. (1999). Forced unfolding of the fibronectin type III module reveals a tensile

- molecular recognition switch. *Proc. Natl. Acad. Sci. USA* 96, 1351–1356.
- Leahy, D.J., Hendrickson, W.A., Aukhil, I., and Erickson, H.P. (1992). Structure of a fibronectin type III domain from tenascin phased by MAD analysis of the selenomethionyl protein. *Science* 258, 987–991.
- Leahy, D.J., Aukhil, I., and Erickson, H.P. (1996). 2.0 Å crystal structure of a four-domain segment of human fibronectin encompassing the RGD loop and synergy region. *Cell* 84, 155–164.
- Lu, H., and Schulten, K. (1999). Steered molecular dynamics simulation of conformational changes of immunoglobulin domain I27 interpret atomic force microscopy observations. *Chem. Phys.* 247, 141–153.
- Lu, H., and Schulten, K. (2000). The key event in force-induced unfolding of Titin's immunoglobulin domains. *Biophys. J.* 79, 51–65.
- Lu, H., Isralewitz, B., Krammer, A., Vogel, V., and Schulten, K. (1998). Unfolding of titin immunoglobulin domains by steered molecular dynamics simulation. *Biophys. J.* 75, 662–671.
- MacKerell, A.D., Bashford, D., Bellot, M., Dunbrack, R.L., Jr., Evansec, J., Field, M.J., Fischer, S., Gao, J., Guo, H., Ha, S., et al. (1998). All-hydrogen empirical potential for molecular modeling and dynamics studies of proteins using the CHARMM22 force field. *J. Phys. Chem. B* 102, 3586–3616.
- Marszalek, P.E., Lu, H., Li, H., Carrion-Vazquez, M., Oberhauser, A.F., Schulten, K., and Fernandez, J.M. (1999). Mechanical unfolding intermediates in titin modules. *Nature* 402, 100–103.
- Meekhof, A.E., Hamill, S.J., Arcus, V.L., Clarke, J., and Freund, S.M. (1998). The dependence of chemical exchange on boundary selection in a fibronectin type III domain from human tenascin. *J. Mol. Biol.* 282, 181–194.
- Nelson, M.T., Humphrey, W., Gursoy, A., Dalke, A., Kale, L.V., Skeel, R.D., and Schulten, K. (1996). NAMD: a parallel, object-oriented molecular dynamics program. *Int. J. Supercomput. Appl.* 10, 251–268.
- Oberdorfer, Y., Fuchs, H., and Janshoff, A. (2000). Conformational analysis of native fibronectin by means of force spectroscopy. *Langmuir* 16, 9955–9958.
- Oberhauser, A.F., Marszalek, P.E., Erickson, H.P., and Fernandez, J.M. (1998). The molecular elasticity of the extracellular matrix protein tenascin. *Nature* 393, 181–185.
- Oberhauser, A.F., Marszalek, P.E., Carrion-Vazquez, M., and Fernandez, J.M. (1999). Single protein misfolding events captured by atomic force microscopy. *Nat. Struct. Biol.* 6, 1025–1028.
- Oberhauser, A.F., Badilla-Fernandez, C., Carrion-Vazquez, M., and Fernandez, J.M. (2002). The mechanical hierarchies of fibronectin observed with single-molecule AFM. *J. Mol. Biol.* 319, 433–447.
- Ohashi, T., Kiehart, D.P., and Erickson, H.P. (2002). Dual labeling of the fibronectin matrix and actin cytoskeleton with green fluorescent protein variants. *J. Cell Sci.* 115, 1221–1229.
- Paci, E., and Karplus, M. (1999). Forced unfolding of fibronectin type 3 modules: an analysis by biased molecular dynamics simulations. *J. Mol. Biol.* 288, 441–459.
- Paci, E., and Karplus, M. (2000). Unfolding proteins by external forces and temperature: the importance of topology and energetics. *Proc. Natl. Acad. Sci. USA* 97, 6521–6526.
- Pankov, R., and Yamada, K.M. (2002). Fibronectin at a glance. *J. Cell Sci.* 115, 3861–3863.
- Park, S., Khalili-Araghi, F., Tajkhorshid, E., and Schulten, K. (2003). Free energy calculation from steered molecular dynamics simulations using Jarzynski's equality. *J. Chem. Phys.* 119, 3559–3566.
- Rofstad, E.K. (2000). Microenvironment-induced cancer metastasis. *Int. J. Radiat. Biol.* 76, 589–605.
- Sachchidanand, Lequin O., Staunton D., Mulloy B., Forster M.J., Yoshida K., and Campbell I.D. (2002). Mapping the heparin-binding site on the 13-14F3 fragment of fibronectin. *J. Biol. Chem.* 277, 50629–50635.
- Schulten, K., Schulten, Z., and Attila, S. (1981). Dynamics of reactions involving diffusive barrier crossing. *J. Chem. Phys.* 74, 4426–4432.
- Sharma, A., Askari, J.A., Humphries, M.J., Jones, E.Y., and Stuart, D.I. (1999). Crystal structure of a heparin- and integrin-binding segment of human fibronectin. *EMBO J.* 18, 1468–1479.
- Steward, A., Adhya, S., and Clarke, J. (2002). Sequence conservation in Ig-like domains: the role of highly conserved proline residues in the fibronectin type III superfamily. *J. Mol. Biol.* 318, 935–940.
- Zhong C.L., Chrzanowska-Wodnicka M., Brown J., Shaub A., Belkin A. M., and Burridge K. (1998). Rho-mediated contractility exposes a cryptic site in fibronectin and induces fibronectin matrix assembly. *J. Cell Biol.* 141, 539–551.